Attenuated Total Reflection Fourier Transform Infrared (ATR FT-IR) Spectroscopy Sensitivity to the Thermal Decay of Bone Collagen

Journal:	*Applied Spectroscopy*
Manuscript ID	ASP-22-0123.R2
Manuscript Type:	Spectroscopic Techniques
Date Submitted by the Author:	13-Sep-2022
Complete List of Authors:	Thomas, Brian; University of Liverpool, Mass Spectrometry Group Anderson, Kevin; Arizona Christian University W. De Silva, Imesha; Lacore Labs Verbeck, Guido; University of North Texas Taylor, Stephen; University of Liverpool, Electrical Engineering and Electronics
Manuscript Keywords:	ATR-IR, Second-harmonic generation imaging, Artificial decay, Collagen
Abstract:	The analysis of collagen stability is of interest in forensics, archaeology, and molecular paleontology. Collagen decay rates are often measured by thermal kinetic studies that employ liquid chromatography mass spectrometry (LC-MS) to assay collagen quantities. However, these kinetic studies generally focus on measuring the decreasing levels of collagen instead of an exact molecular concentration of each sample. Thus, attenuated total reflection Fourier-transform infrared (ATR-FTIR) spectroscopy can offer a simpler and less expensive alternative to LC-MS. The application of a new protocol to determine decreasing amounts of bone collagen in artificially decayed porcine and bovine bone was assessed. The protocol uses a forensic application of ATR-FTIR spectroscopy on size-restricted bone powder from three uniformly high temperature conditions. Also for the first time, collagen-specific second-harmonic generation (SHG) imaging was also applied to artificially aged bone to add an independent, qualitative perspective to parallel FTIR assessments. SHG images and ATR-FTIR spectra together reveal the same orderly bone collagen decay as found in previous thermal kinetic studies. Resulting Arrhenius plots with r2 values > 0.95 suggest that the ATR-FTIR-based protocol has potential as a precise and simple tool for measuring bone collagen decay rates. The results are significant for applications of thermal kinetic studies, and our protocol can serve as an inexpensive, precise, and pragmatic means of evaluating bone collagen stability within an array of conditions.

ATR-FTIR Spectroscopy is Sensitive to Thermal Decay of Bone Collagen

Brian Thomas*
Electrical Engineering and Electronics
University of Liverpool
Brownlow Hill
Liverpool
L69 7ZX
brian.thomas@liv.ac.uk

Kevin Anderson
Department of Biology
Arizona Christian University
Glendale, AZ
anderson@arizonachristian.edu

Imesha De Silva
Department of Chemistry
University of North Texas
Denton, TX
imesha_gim@yahoo.com

Stephen Taylor
Electrical Engineering and Electronics
University of Liverpool
Brownlow Hill
Liverpool
L69 7ZX
s.taylor@liv.ac.uk

* corresponding author

Declaration of Interest: None

Abstract (222)

The analysis of collagen stability is of interest in forensics, archaeology, and molecular paleontology. Collagen decay rates are often measured by thermal kinetic studies that employ liquid chromatography mass spectrometry (LC-MS) to assay collagen quantities. However, these kinetic studies generally focus on measuring the decreasing levels of collagen instead of an exact molecular concentration of each sample. Thus, attenuated total reflection Fourier-transform infrared (ATR-FTIR) spectroscopy can offer a simpler and less expensive alternative to LC-MS. The application of a new protocol to determine decreasing amounts of bone collagen in artificially decayed porcine and bovine bone was assessed. The protocol uses a forensic application of ATR-FTIR spectroscopy on size-restricted bone powder from three uniformly high temperature conditions. Also for the first time, collagen-specific second-harmonic generation (SHG) imaging was also applied to artificially aged bone to add an independent, qualitative perspective to parallel FTIR assessments. SHG images and ATR-FTIR spectra together reveal the same orderly bone collagen decay as found in previous thermal kinetic studies. Resulting Arrhenius plots with r^2 values > 0.95 suggest that the ATR-FTIR-based protocol has potential as a precise and simple tool for measuring bone collagen decay rates. The results are significant for applications of thermal kinetic studies, and our protocol can serve as an inexpensive, precise, and pragmatic means of evaluating bone collagen stability within an array of conditions.

Key Words

ATR-FTIR; Fourier transform infrared spectroscopy; Second harmonic generation; Collagen degradation; Thermal kinetics

1. Introduction

Collagen is the most common structural protein in vertebrates. The collagen family of proteins comprises the majority of the total organic content of bone. It contains a high content of glycine, proline, and hydroxyproline, usually in a repeated -gly-pro- hypro-gly- pattern [1]. This arrangement of relatively small residues permits the coiled architecture of each subunit. The flexibility of this fibrous biomolecule provides bone its resilience, while the rigid structure of biomineral components provides compressive resistance [2].

The abundance of collagen, its insolubility in water, resistance to degradation, and ability to be separated from calcium hydroxyapatite makes it an ideal bone component for radiocarbon and stable isotope analysis [3]. Since its introduction in 1977, stable isotope analysis of bone collagen has been widely used to reconstruct aspects of early human and animal diets [4, 5]. Collagen content is also used for forensic investigation [6] and species identification in archaeological settings [7]. Collagen fragments have even been detected in some palaeontological specimens [8].

Each of these applications is impacted by conditions affecting collagen integrity and decay. Thermal kinetic studies have proven useful for answering questions about collagen stability in relationship to environmental conditions. For example, Collins et al modeled bone collagen decay as a temperature-dependent first order reaction of hydrolytic cleavage of peptide bonds [9]. Experiments that artificially decay bone under ideal conditions have been used to generate thermal “ages” for archaeological bone samples [10]. Our approach follows these demonstrations of artificial decay as idealized diagenesis of buried bone.

However, such kinetic studies typically employ liquid chromatography mass spectrometry (LC-MS) for quantifying bone collagen. This approach is often limited by the expense and technical challenges in operation and maintenance of the equipment. Bone sample preparation also involves some form of collagen extraction, which can reduce analytical precision [11-13]. In addition, many chemical quantification kits for bone collagen (e.g., Sirius Red) also rely on sample extraction protocols that depend on variability of extraction yields [14].

Thus, the costs and technical challenges associated with LC-MS can limit the variety and extent of thermal kinetic studies. This limitation may be a constraining factor in our understanding of bone collagen stability. Plus, these kinetic studies focus more on precisely measuring the change of collagen levels over time, rather than the specific molecular concentration of each sample. Therefore, Fourier transform infrared (FTIR) spectroscopy offers a lower cost and maintenance alternative to LC-MS, which could make kinetic studies more tractable. In turn, this could expand the utility of such studies, enabling a greater understanding of factors effecting collagen stability.

FTIR is used in an increasing number of applications as a rapid and inexpensive technique to assess the presence and quantity of organic molecules. It shows high sensitivity to vibrational modes of organic functional groups [15, 16]. For example, FTIR was recently evaluated as a tool for prescreening archaeological bone samples for the presence of collagen [17], and as a forensic test for the detection of collagen remnants in burned bone remains [18, 19]. Our prior work used FTIR and protein sequencing by MS to establish the applicability of Second Harmonic Generation imaging to study medieval and even Pleistocene bone collagen remnants [20]. Other studies have used FTIR spectroscopy to map Mesozoic bone collagen [21]. FTIR showed sensitivity to human bone amide bond decay with increasing age-at-death, suggesting its sensitivity to further degradation post-mortem[22]. FTIR may thus be useful in not only examining ancient bone, but also in characterizing bone collagen diagenesis.

We sought to assess if a protocol employing FTIR could be adapted for thermal kinetic studies. To this end, FTIR spectra were collected from artificially decayed modern porcine and bovine bone. Using two types of bone allowed the sensitivity and precision of the technique to be tested for two bone types with decreasing levels of bone collagen. This allowed us to explore the potential of FTIR for labor and cost savings.

Thompson et al [19] found that using carbonyl-to-phosphate peak height (C=O/PO_4, herein CO/P) ratios afford a semiquantitative measurement, since carbonyl moieties from the organic bone fraction diminish during decay while the phosphates from the mineral fraction do not. Those authors associated the carbonyl moiety within the amide amide I bond peak

at approximagely 1650 cm-1. Second, we considered that air temperatures in various locations within a dry oven would decrease the uniformity of decay rates across samples and thus decrease overall precision. To remedy this, bone powder and shards were immersed in water baths for the first time and each maintained at constant temperature. Last, Kontopoulos et al [23] found systematic IR peak shifts with grain size differences and demonstrated procedures including multiple sampling runs and the use of uniform grain sizes to mitigate these effects. Sieves were therefore used in preparation for FTIR measurements. This new protocol thus brings together for the first time the collection of C=O/P peak height ratios from Thompson et al, triplicate measurements of specified grain-sizes of powderized bone from Kontopoulos et al, and exposure to uniformly high temperatures by use of water baths used to construct Arrhenius plots, as per Collins and co-workers [24].

In addition, SHG imaging is a non-destructive microscopic technique that can optically examine fibrillar collagen in bone and other tissues [25]. SHG captures endogenous highly structural proteins and, in common with multiphoton excited fluorescence, reveals intrinsic three-dimensionality [26]. We used SHG as a visual and qualitative confirmation of the quantitative bone collagen fiber decay rates obtained using FTIR. SHG images have the potential to quantify collagen whole fibers, which range from 0.3-300 µm in diameter [27], whereas FTIR may detect more highly degraded, smaller proteinaceous remnants although at a limited spatial resolution, dependent on the specific sampling approach.

Decay of organic materials including collagen and other protiens is attracting interest due to the presence of these materials in biomineralised remains of organisms from forensic, archaeologica, and even geologic specimens [28]. Our studies are aimed at helping answer questions of collagen stability in different settings by establishing standardized protocols for characterizing levels of bone collagen decay.

2. Materials and Methods

2.1 Bone Preparation

An artificial bone decay protocol was developed based on the methods used by Collins et al [9] and Dobberstein et al [29]. Porcine and bovine metacarpal and metatarsal bones were obtained from a local market. Bones were hand-cleaned of all muscle and connective tissue. Portions of the bone were then air dried, mechanically crushed, and further ground to a powder measuring between 500 µm and 250 µm in granule size. In addition, small shards (~5 x 20 x 2 mm) of cortical bone fragments were broken from the same cleaned porcine and bovine bones for SHG Imaging.

2.2 Thermal Kinetic Experiments

The near-term objective was to establish a protocol that reliably measures bone collagen integrity in artificial decay experiments. Once in place, future studies can use this protocol to build collagen decay kinetics models for use in archaeology and even paleontology. Additional future studies could use this protocol to test conditions that may affect collagen longevity.

Approximately 2 g of either porcine or bovine bone powder (500 µm - 250 µm granule size) were separately placed into 25 ml ampules (Wheaton, Millville, NJ). Preliminary work revealed that more consistent results were obtained when larger grain sizes (500-250 µm) were used during the high temperature incubation period. A single bone shard was also placed into each ampule. The bone powder and shard were saturated with deionized water (HPLC grade; Fisher Scientific), after which the ampules were placed into an 80°C water bath and held for 30 minutes. Excess water was then decanted from the ampules, leaving a moist, granular bone sample.

Ampules were heat-sealed and placed into water baths maintained at 82° C, 86° C, and 90° C for porcine bone, and 80° C, 85° C, and 90° C for bovine bone. Two ampules were subsequently removed from each water bath according to a preset sampling schedule. These ampules were then opened and bone content drained onto a Falcon cell strainer (40 µm) and air-dired at STP. These samples were further ground to a final size restriction of 62-20 µm by sifting with stacked sieves (Cole Parmer). The resulting bone powder was stored at 4°C until used for FTIR analysis. Bone shards were removed from the powdered bone and individually stored at 4°C for SHG microscopy.

2.3 ATR-IR Spectroscopy

Collagen content of individual powdered bone samples was determined using a FTIR Spectrometer (Thermo Scientific Nicolet 6700) with the Smart iTX modular ~~multiple~~single-bounce diamond ATR accessory. Preliminary results show~~s~~ that the irregular surface of bone shards produced irregular spectra using the ATR. In contrast to such shards, the highly polished bone surfaces of thinsections as prepared for microscopy can be suitable for reliable FTIR results. However, the intense labor and expertise required to make thinsections make it impractical for the high volume of samples used in this study and for the potential of portability emphasized here. Thus, bone powder wa~~i~~s ~~required~~ selected for this technique, whereas whole bone shards were ~~required~~ used for the visualization described below.

We performed triplicate FTIR scanning of each replicated sample, as suggested by Kontopoulos et al [23], which helps ensure uniform spectra. This totaled 135 spectra for each bone type at all three temperatures. The diamond window sampling area of the Nicolet 6700 is 3 mm in diameter. Omnic software was used to record spectra over the wavenumber range 500 cm^{-1} to 4000 cm^{-1} at a spectral resolution of 4 cm^{-1}. An individual spectrum represented an average of 16 scans, and spectra were saved as .csv files.

The “find peaks” function in Omnic was used to determine peaks from each resulting spectrum. The tolerance slider was adjusted just until the software displayed the carbonyl (C=O) peak at ~1650 cm^{-1}. This procedure also captured the phosphate (PO_4) peak of interest, which was always much larger. Since the goal was to test the reliability of ATR-IR method with as few manipulations as reasonably possible, spectra were not baselined. Results, for example R-values for decay plots, thus reflect raw spectra. Further, in the regions where peak heights were assessed the baseline on either side of each peak was flat. Ensuring a flat raw baseline required periodically baselining the instrument, recleaning the window, and re-measuring the sample.

C=O and PO_4 peak intensities for all six reads (three reads of each replication) were averaged for every temperature and time. These averages were used to construct an

Arrhenius plot as per Collins and coworkers [30]. The slope of the line of best fit calculated for the C=O/P ratio versus time (days) was used for the rate constant (k) for each of the three temperatures, following k = -slope. The Arrhenius plot places k on the Y axis and the inverse temperature (°K) on the X axis to generate an activation energy and pre-exponential factor that the Arrhenius equation requires to determine collagen decay kinetics.

2.4 Second Harmonic Generation (SHG)

Collagen content of selected, incubated bone shards was also visualized by second-harmonic generation microscopy (SHG) in order to qualitatively verify the FTIR-based quantification. SHG imaging was performed as previously described [20]. Bone shards were mounted on glass slides and imaged under a Zeiss Plan-Apochromat 10×, NA =0.45 objective lens using a Zeiss Examiner Z1 two-photon excitation laser scanning confocal microscope (Carl Zeiss, Jena, Germany) coupled to a Coherent Chameleon titanium:sapphire laser (Coherent, Glasgow, UK). The laser was set to 920 nm for excitation. The SHG emission signal was collected at 458 nm (half the excitation wavelength).

A parallel autofluorescent signal was also collected at 760 nm. Cellular components including lipopigments and vitamin derivatives [31] as well as aromatic amino acids [32] will autofluoresce. Inclusion of these components in a parallel image provides a context for comparison with the collagen histology. A dual channel Zeiss LSM BiG detector captured both the SHG and autofluorescent channels simultaneously. Focal planes and bone regions were selected to include sufficient collagen to visualize within the viewing frame.

In highly decayed samples, the collagen diminished until their SHG signal lost some visual context. Therefore, a separate reflectance image was collected over the same viewing area using a 561nm laser at 6.9mW power. The pinhole aperture was set to its widest setting, which spanned 79.3 µm, and the detector range spanned 415-735nm. These settings allowed a widefield image that captured the uppermost bone surface. Overlays show collagen remnants in the context of the rough bone contours. Frame sizes of 1932 × 1932 pixels were rastered at 5 s speed, taking the average of four reads per line.

Open source ImageJ software package Fiji [33] was used to overlay parallel channels and adjust channel brightness. Intensity thresholds were set to 40–255 to visualize the strong and broad collagen signal seen in fresh bone, and they were set to 20 to 255 to visualize the faint and spotty signal seen in artificially decayed bone.

3. Results and Discussion

A novel protocol using FTIR was assessed for its utility in thermal kinetic studies of bone collagen. The use of CO/P ratios quantified collagen decay results. Standardizing bone particle size produced uniform spectra and thus directly comparable CO/P ratios. These comparable ratios provided measurements that monitor changes to bone collagen concentration. Since the infrared light interacts directly with the bone samples, this protocol does not require chemical extraction procedures, thereby reducing inconstancies introduced by variances in extract efficiency. The use of water baths provided more uniform experimental incubation temperatures that help contribute to resulting uniformity of data, effectively decreasing scatter in Arrhenius plot experimentss that used ovens, such as in Collins et al, 2000 [24].

Certain of the representative specra in Figures 3 and 4 have a peak or an inverse peak at approximately 1150 cm-1. This variability was found to be due to propellant used to clean the ATR surface. Several samples were therefore reanalyzed after the propellant evaporated and resulting spectra were compared to those that had already been collected. No difference in CO/P ratios were found between the two, thus establishing that the intruding substance did not affect results.

The measured collagen content for each sample was plotted vs time for the three experimental temperatures (Fig 1a and 2a). This resulted in three separate plotted lines for each bone. Slopes from the three plots were used to obtain a best fit regression (Fig. 1b and Fig 2b). The regression value for porcine bone was $r^2 = 0.99$ and $r^2 = 0.95$ for bovine bone.

Bovine and porcine bone tissues have several compositional differences, including lipid content and bone density [34, 35]. Using both bone types in this study helped us evaluate

any compositional effect on the FTIR analysis. Different temperature ranges for the decay of the two bone types were used in order to refine the proficiency of experimental procedures. The high r^2 value of both bone/temperature combinations revealed that these differences did not appreciably affect overall results.

High r^2 values of the regressions illustrate the reliability of this new protocol as a highly precise methodology for direct assessment of bone collagen integrity. In particular, we found that FTIR provides results with the precision necessary for use in thermal kinetic studies of bone collagen.

Figures 3 and 4 include representative FTIR spectra from selected temperature runs. Some spectra show either a peak or negative peak at ~1150 cm-1. This was attributed to propellant used to clean the window between scans. Scores of scans with or without the propellant did not affect the C=O peak. Once deduced, use of the propellant was discontinued. These figures show in essence a diminishing C=O peak height over time. We interpret this trend as being consistent with the chemical hydrolysis that Collins et al referred to as “Mechanism 1” of collagen loss in buried bone[3]. Water was present in the sealed ampules, even as it is present underground, and thus available for chemistry. Carbonyl moieties are susceptible to electrophilic attack, so that amide bond loss through hydrolysis reasonably accounts for the systematic C=O peak decline in our results shown in Figures 1 and 2.

As a complement to FTIR, SHG was used to obtain a confirmatory qualitative assessment of collagen decay. We had previously used SHG to investigate the presence of collagen in modern, medieval and ancient (including fossil bone) [20]. In that study, collagen presence was independently confirmed using MS sequencing, FTIR, and Raman spectroscopy. The SHG signal shown in red in Figures 3 and 4 revealed a steady decline of collagen over time with respect to temperature. The logarithmic character of this decline, as illustrated with porcine bone (Fig 3) and bovine bone (Fig 4) appears visually consistent with that quantified by FTIR and shown in Figures 2 and 1, respectively. The SHG images also provide information on the spatial distribution of bone collagen remnants, which could be used for future studies that compare artificial with actual collagen decay characteristics.

4. Conclusions

We tested a unique protocol featuring an FTIR application to thermal kinetic studies. The protocol involved collagen quantification through CO/P ratios, uniformity of experimental temperatures through use of water baths, and uniformity of spectral characters through bone-powder size selection. This protocol offers a less costly and less technically demanding means to monitor changes in quantity of bone collagen than more commonly used protocols. SHG imaging visually confirmed the decline of bone collagen as measured by our protocol. Thus, the high precision of the FTIR data suggests our protocal can serve as a user- friendly, yet qualitatively-suitable means of employing thermal kinetic studies to assess bone collagen decay rates.

In future experiments we envisage adding other chemicals, e.g. iron and various buffers, to the sealed bone shards and/or powdered bone to investigate their effects on bone collagen decay rates. Both bone preparations are achievable in the field for immediate analysis. Furthermore, use of portable techniques such as FTIR are currently of interest for on-site archaeology in the context of estimating bone ages relative to thermal or “collagen” age plots such as that of Buckley and Collins [10].

Our experiments, though numerous, were conducted at a relatively high temperature of 80C - 90C. Although this shortens the incubation time, it may decrease accuracy. Therefore, reproduction of our results at lower temperatures is of interest and the subject of current research. This approach may also help assess whether other degradation mechanisms with differing reaction kinetics come into play at lower temperatures.

Acknowledgments

We thank Joshua Jacobi and Ryan Anderson for their assistance in the laboratory. Abhi Bugde and Kate Phelps of the Live Cell Imaging Core Facility at UT Southwestern Medical Center assisted with SHG imaging, supported by NIH S10 RR029731-01. We specially thank

Tom Kiselak from Guido Verbeck's Laboratory of Imaging Mass Spectrometry at the University of North Texas for their assistance with ATR-IR.

References

1. **W. Yang, V. C. Chan, A. Kirkpatrick, J. A. Ramshaw, and B. Brodsky**, J Biol Chem, **272**, 46, 28837-28840 (1997).
2. **D. Shier, Butler, J., and Lews, R.** , *Holes' Human Anatomy and Physioolgy, Tenth Edition* (McGraw Hill, New York, 2004).
3. **M. J. Collins, Nielsen-Marsh, C.M., Hiller, J., Smith, C.I., Roberts, J.P., Prigodich, R.V., Wess, T.J., Csapo, J., Millard, A.R., and Turner-Walker, G.**, Archaeometry, **44**, 3, 383-394 (2002).
4. **N. J. Van der Merwe and J. C. Vogel**, Nature, **276**, 5690, 815-816 (1978).
5. **J. C. Vogel and N. J. Van Der Merwe**, American Antiquity, **42**, 2, 238-242 (1977).
6. **K. Jellinghaus, P. K. Urban, C. Hachmann, M. Bohnert, G. Hotz, W. Rosendahl, and U. Wittwer-Backofen**, Legal Medicine, **36**, 96-102 (2019).
7. **M. Buckley, M. Collins, J. Thomas-Oates, and J. C. Wilson**, Rapid Commun Mass Spectrom, **23**, 23, 3843-3854 (2009).
8. **E. R. Schroeter, C. J. DeHart, T. P. Cleland, W. Zheng, P. M. Thomas, N. L. Kelleher, M. Bern, and M. H. Schweitzer**, J Proteome Res, **16**, 2, 920-932 (2017).
9. **M. J. Collins, Riley, M.S., Child, A.M., Turner-Walker, G.**, J. Archaeol. Sci., **22**, 175–183 (1995).
10. **M. Buckley and M. J. Collins**, Antiqua, **1**, 1, e1 (2011).
11. **M. Harbeck and G. Grupe**, Archaeological and Anthropological Sciences, **1**, 1, 43-57 (2009).
12. **J. Sealy, M. Johnson, M. Richards, and O. Nehlich**, Journal of Archaeological Science, **47**, 64-69 (2014).
13. **C. Wadsworth and M. Buckley**, Rapid Communications in Mass Spectrometry, **28**, 6, 605 (2014).
14. **E. R. Schroeter, C. J. DeHart, M. H. Schweitzer, P. M. Thomas, and N. L. Kelleher**, PeerJ, **4**, e2603 (2016).
15. **S. E. Glassford, B. Byrne, and S. G. Kazarian**, Biochim Biophys Acta, **1834**, 12, 2849-2858 (2013).
16. **Z. Movasaghi, S. Rehman, and D. I. ur Rehman**, Applied Spectroscopy Reviews, **43**, 2, 134-179 (2008).
17. **M. Lebon, I. Reiche, X. Gallet, L. Bellot-Gurlet, and A. Zazzo**, Radiocarbon, **58**, 1, 131-145 (2016).
18. **T. Thompson, M. Gauthier, and M. Islam**, Journal of Archaeological Science, **36**, 3, 910-914 (2009).
19. **T. Thompson, M. Islam, and M. Bonniere**, Journal of Archaeological Science, **40**, 1, 416-422 (2013).
20. **B. Thomas, D. McIntosh, T. Fildes, L. Smith, F. Hargrave, M. Islam, T. Thompson, R. Layfield, D. Scott, and B. Shaw**, Bone reports, **7**, 137-144 (2017).
21. **Y. C. Lee, C. C. Chiang, P. Y. Huang, C. Y. Chung, T. D. Huang, C. C. Wang, C. I. Chen, R. S. Chang, C. H. Liao, and R. R. Reisz**, Nat Commun, **8**, 14220 (2017).
22. **J.-M. Very, R. Gibert, B. Guilhot, M. Debout, and C. Alexandre**, Calcified tissue international, **60**, 3, 271-275 (1997).
23. **I. Kontopoulos, S. Presslee, K. Penkman, and M. J. Collins**, Vibrational Spectroscopy, (2018).

24. **M. J. Collins, A. M. Gernaey, C. M. Nielsen-Marsh, C. Vermeer, and P. Westbroek**, Geology [Boulder], **28**, 12, 1139-1142 (2000).
25. **X. Chen, O. Nadiarynkh, S. Plotnikov, and P. J. Campagnola**, Nat Protoc, **7**, 4, 654-669 (2012).
26. **W. Mohler, A. C. Millard, and P. J. Campagnola**, Methods, **29**, 1, 97-109 (2003).
27. **N. Naik, J. Caves, E. L. Chaikof, and M. G. Allen**, Adv Healthc Mater, **3**, 3, 367-374 (2014).
28. **B. Thomas and S. Taylor**, Expert review of proteomics, **16**, 11-12, 881-895 (2019).
29. **R. C. Dobberstein, Collins, M.J., Craig, O.E., Taylor, G., Penkman, E.E.H., Ritz-Timme, S.**, Archaeological and Anthropological Science, **1**, 1, 31-42 (2009).
30. **G. D. Cody, N. S. Gupta, D. E. G. Briggs, A. L. D. Kilcoyne, R. E. Summons, F. Kenig, R. E. Plotnick, and A. C. Scott**, Geology, **39**, 3, 255-258 (2011).
31. **W. R. Zipfel, R. M. Williams, R. Christie, A. Y. Nikitin, B. T. Hyman, and W. W. Webb**, Proc Natl Acad Sci U S A, **100**, 12, 7075-7080 (2003).
32. **M. Monici**, Biotechnol Annu Rev, **11**, 227-256 (2005).
33. **J. Schindelin, I. Arganda-Carreras, E. Frise, V. Kaynig, M. Longair, T. Pietzsch, S. Preibisch, C. Rueden, S. Saalfeld, and B. Schmid**, Nature methods, **9**, 7, 676 (2012).
34. **J. Aerssens, S. Boonen, G. Lowet, and J. Dequeker**, Endocrinology, **139**, 2, 663-670 (1998).
35. **R. A. Field, M. Riley, F. Mello, J. Corbridge, and A. Kotula**, Journal of Animal Science, **39**, 3, 493-499 (1974).

List of figures

Figure 1. Arrhenius plots for bovine bone collagen concentration from FTIR spectra. Three decay plots show bovine bone collagen loss over time for each of three temperatures. The slope of each was used to construct an Arrhenius plot, a regression plot of Ln(CO/P) and inverse temperature in°K. The result shows a high r2 = 0.95 that reflects precision of our FTIR-based protocol.

Figure 2. Arrhenius plots for porcine bone collagen concentration from FTIR spectra. Three decay plots show porcine bone collagen loss over time for each of three temperatures. The slope of each was used to construct an Arrhenius plot, a regression plot of Ln(CO/P) and inverse temperature in°K. The result shows a high r2 = 0.999 that reflects precision of our FTIR-based protocol.

Figure 3. Representative FTIR spectra and corresponding SHG images for six selected days of artificial porcine bone collagen decay at 82°C. CO/P averages were calculated from six scans—three measurements for each of two experimental replications. One representative scan from those six is shown. The use of peak assignments for phosphate (~1025 cm-1) and collagen-specific carbonyl (~1650 cm-1) was taken from Thompson, Islam, and Bonniere, 2013 [15]. The red SHG signal diminishes parallel to the apparent carbonyl peak height depletion over time. SHG images of collagen were assigned red, and autofluorescencing bone organics assigned to green. Signal intensity thresholds for each channel were adjusted to maintain visibility as the red signal diminished with

collagen decay over time. Day 0 shows fresh, unheated bone at a signal threshold of 0-75 with green signal threshold at 0-

145. Day 4 shows the SHG red signal threshold at 0-75 with green threshold at 0-145. Day 6 shows the red threshold at 0-75 with green signal threshold at 5-200. Day 10 shows red signal threshold at 0-75 with green signal threshold at 0-145. Day 14 shows red signal threshold at 0-75 with gray reflectance at 0-145.

Figure 4. Representative FTIR spectra and corresponding SHG images from five selected days of artificial bovine bone collagen decay at 90˚C. Apparent carbonyl peak height lowers as apparent red SHG signal diminishes over time. SHG images of collagen were assigned red, and autofluorescening bone organics assigned to green. For Days 6, 11, and 14, a reflectance image overlay was used to show the total area of bone in focus during SHG image collection, since autofluorescent (green) signal had disappeared by then. Signal intensity thresholds were adjusted as follows: Day 1 shows the red signal threshold after 24h of incubation at 90˚C at 0-200 with green signal threshold at 0-100. Day 3 shows the SHG red signal threshold at 0-200 with green threshold at 0-200. Day 6 shows the red threshold at 0-100 with gray reflectance threshold at 75-255. Day 10 shows red signal threshold at 0-125 with gray reflectance at 100-350. Day 14 shows red signal threshold at 0- 125 with gray reflectance at 75-305.

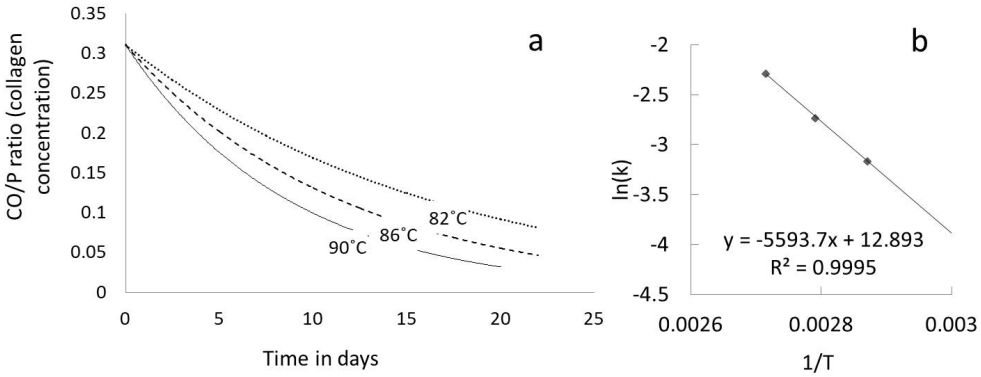

Arrhenius plots for bovine bone collagen concentration from FTIR spectra. Three decay plots show bovine bone collagen loss over time for each of three temperatures. The slope of each was used to construct an Arrhenius plot, a regression plot of Ln(CO/P) and inverse temperature in K. The result shows a high r2 = 0.95 that reflects precision of our FTIR-based protocol.

243x99mm (150 x 150 DPI)

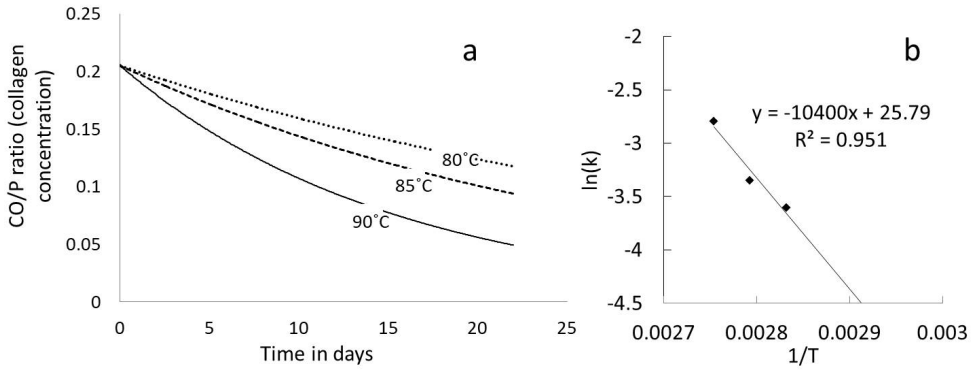

Arrhenius plots for porcine bone collagen concentration from FTIR spectra. Three decay plots show porcine bone collagen loss over time for each of three temperatures. The slope of each was used to construct an Arrhenius plot, a regression plot of Ln(CO/P) and inverse temperature in K. The result shows a high r2 = 0.999 that reflects precision of our FTIR-based protocol.

249x102mm (150 x 150 DPI)

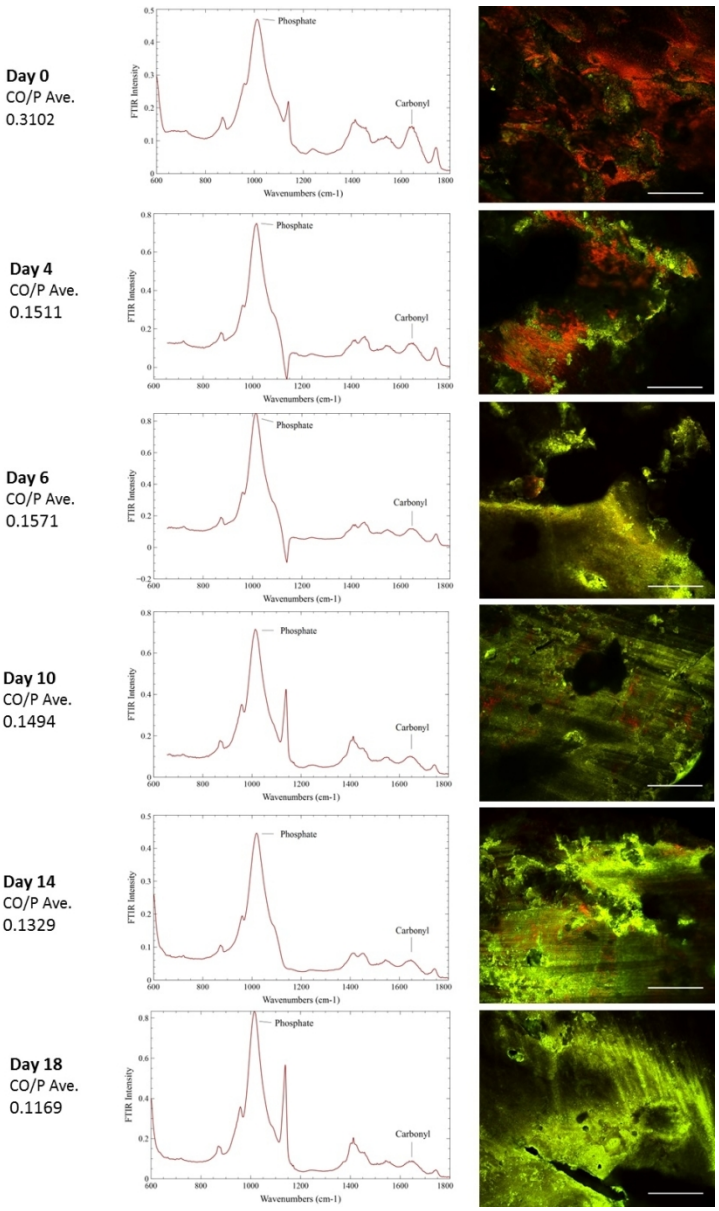

256x424mm (96 x 96 DPI)

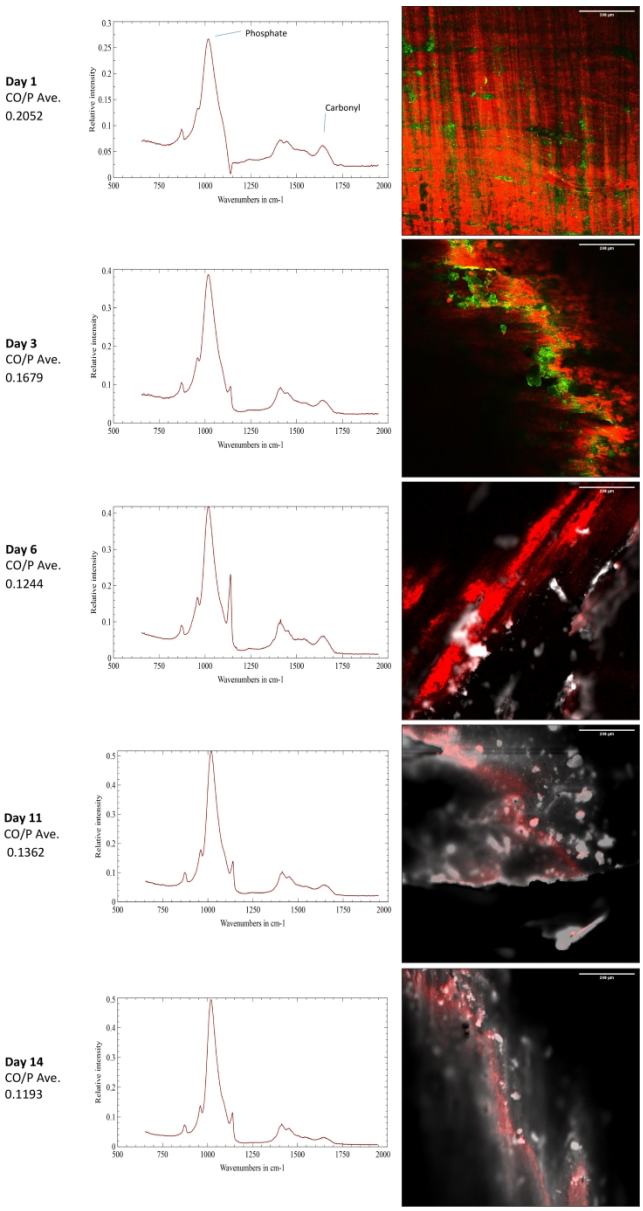

Representative FTIR spectra and corresponding SHG images from five selected days of artificial bovine bone collagen decay at 90 C. Apparent carbonyl peak height lowers as apparent red SHG signal diminishes over time. SHG images of collagen were assigned red, and autofluorescening bone organics assigned to green. For Days 6, 11, and 14, a reflectance image overlay was used to show the total area of bone in focus during SHG image collection, since autofluorescent (green) signal had disappeared by then. Signal intensity thresholds were adjusted as follows: Day 1 shows the red signal threshold after 24h of incubation at 90 C at 0-200 with green signal threshold at 0-100. Day 3 shows the SHG red signal threshold at 0-200 with green threshold at 0-200. Day 6 shows the red threshold at 0-100 with gray reflectance threshold at 75-255. Day 10 shows red signal threshold at 0-125 with gray reflectance at 100-350. Day 14 shows red signal threshold at 0- 125 with gray reflectance at 75-305.

177x333mm (300 x 300 DPI)

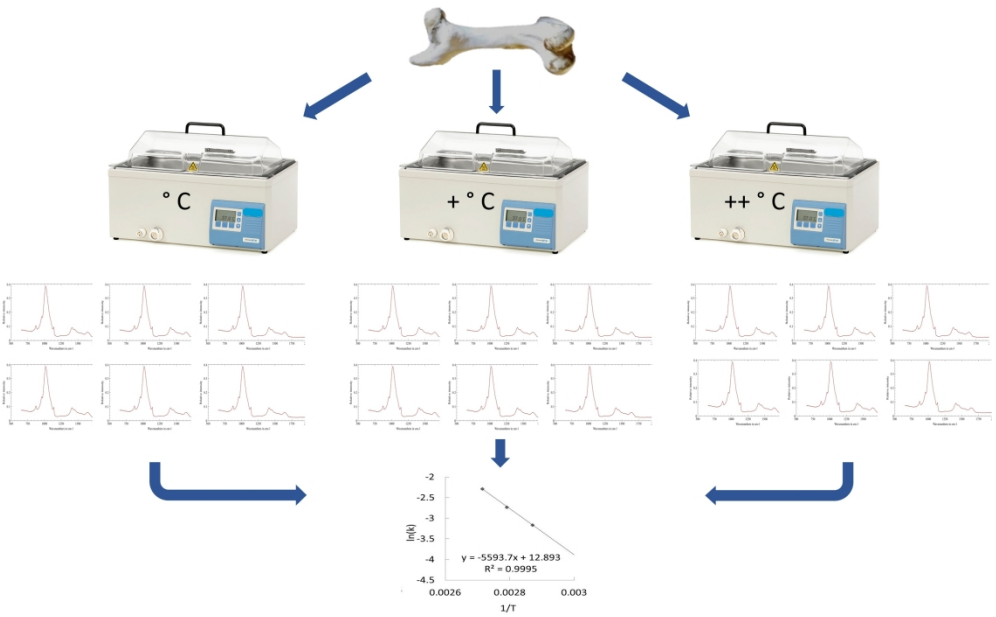

922x564mm (96 x 96 DPI)